Helical Foldamer Channels

International Edition: DOI: 10.1002/anie.201906341
German Edition: DOI: 10.1002/ange.201906341

# Pyridine/Oxadiazole-Based Helical Foldamer Ion Channels with Exceptionally High $K^+/Na^+$ Selectivity

*Feng Chen, Jie Shen, Ning Li, Arundhati Roy, Ruijuan Ye, Changliang Ren, and Huaqiang Zeng**

***Abstract:*** *Protein channels are characterized by high transport selectivity, which is essential for maintaining cellular function. Efforts to reproduce such high selectivity over the past four decades have not been very successful. We report a novel series of aromatic foldamer-based polymeric channels where the backbone is stabilized by differential electrostatic repulsions among heteroatoms helically arrayed along the helical backbone. Nanotubes averaging 2.3 and 2.7 nm in length mediate highly efficient transport of $K^+$ ions as a consequence of hydrophilic electron-rich hollow cavities that are 3 Å in diameter. Exceptionally high $K^+$ and $Na^+$ selectivity values of 16.3 and 12.6, respectively, are achieved.*

A hallmark of protein channels is their high selectivity in transporting related species across cellular membranes via evolutionarily selected transmembrane pathways. Some notable examples include aquaporins that are super permeable to water molecules ($10^9$ molecules per second) but strictly prevent the passage of ions and even protons,[1a–c] the $K^+$-channel KcsA that displays a $K^+/Na^+$ selectivity of $10^4$,[1d] and the M2 proton channel that is at least $10^5$-fold more selective for protons over other monovalent cations.[1e] These extraordinarily high transport selectivities are crucial for proper cellular functions, including maintaining an ion concentration gradient, regulating membrane potential, and so on; however, they are extremely difficult to replicate in artificially developed species-transporting channels.[2] For instance, despite great efforts to develop synthetic $K^+$-selective channels,[2g,h,3] the highest unambiguously determined $K^+/Na^+$ selectivity of 9.8 was achieved in synthetic channel systems only very recently by a combinatorial screening method.[3i] Other demonstrated $K^+$-selective ion channels include crown ethers conjugated to (thio)urea groups that were developed by Barboiu,[3f,g,j] a pore-forming helical oligomer by Dong,[3h] and a pillararene–cyclodextrin hybrid channel by Xin.[3k]

Aromatic foldamers[2j,k,4] are a class of folding molecules that mostly fold into a crescent-shaped or helically folded structure via non-covalent forces; including, H-bonding,[5a–c] solvophobic forces,[5d,e] and electrostatic repulsions.[3h,5f–j] Helically folded foldamers are additionally stabilized by extensive π–π stacking forces. Intensive research over the past two decades has culminated in a long list of diversified structural codons, enabling the enclosed cavity to be tuned from 2.8 Å[5k] to 30 Å,[5l] or beyond. One unique feature associated with aromatic foldamers, but not commonly seen in other types of supramolecular materials, is the high predictability of the folded structures and cavity sizes, which is derived from their constituent codons. This allows a range of functions to be readily and often predictably integrated into the sequence design of the cavity-containing folded structures.

Nevertheless, despite considerable contributions from the group of Huc et al.,[4d] functional investigations on these aromatic foldamers have been limited to short oligomers of $<1$ nm in helical height because the multistep iterative preparation of foldamers with a long covalent helical backbone is synthetically challenging. If longer tubular foldamers can be efficiently prepared from their constituent repeating units by such as one-pot polymerization,[6a] the corresponding functions can be expanded. As far as aromatic foldamers are concerned, one-pot polymerization has thus far yielded long helical channels of $>2$ nm for only four types of aromatic foldamers stabilized by either electrostatic repulsions[5h,j] or solvophobic forces.[6b,c]

Herein, we report a one-pot polymerization method that successfully delivers aromatic foldamer-based channels with a tubular backbone of 3 Å in diameter and up to 2.7 nm in average helical height (for a representative structure, see the 1.7 nm long $\mathbf{P_{17}}$ in Figures 1 a,b). We also demonstrate that these long foldamer channels with an electron-rich narrow cavity allow ion transport across the membrane with high $K^+/Na^+$ selectivity of 16.3 when a voltage is applied.

The helically folded backbone of $\mathbf{P_n}$ where n refers to the average number of building blocks (Figure 1 a) is stabilized by the differential repulsive forces among heteroatoms, a concept first proposed by Lehn and co-workers[5f–h] and later expanded by Dong.[3h,5i,j] Computationally, the conformer containing alternatively arrayed N and O atoms (as seen in $\mathbf{P_n}$) is 6.31 kcal mol$^{-1}$ more stable than the conformer with all N atoms pointing inward toward the interior (Figure S1). Further high-level computations show that folded $\mathbf{P_n}$ possesses a highly hydrophilic electron-rich hollow cavity that is 3 Å in diameter after subtracting the van der Waals radii of O (1.52 Å) and N (1.55 Å) atoms (Figure 1 c), suggesting that the channels of $\mathbf{P_n}$ may bind to $K^+$ (2.76 Å) more tightly than to $Na^+$ (2.04 Å), and ion transport selectivity is thus expected. Indeed, our computational results reveal the ability of helically arranged O and N atoms in $\mathbf{P_9}$ to provide a sufficient

[*] Dr. F. Chen, Dr. J. Shen, Dr. N. Li, Dr. A. Roy, Dr. C. Ren, Dr. H. Zeng
The NanoBio Lab
31 Biopolis Way, The Nanos, Singapore 138669 (Singapore)
E-mail: hqzeng@nbl.a-star.edu.sg
R. Ye
Department of Chemical and Biomolecular Engineering
National University of Singapore
Singapore 117585 (Singapore)
Supporting information and the ORCID identification number(s) for the author(s) of this article can be found under: https://doi.org/10.1002/anie.201906341.

  

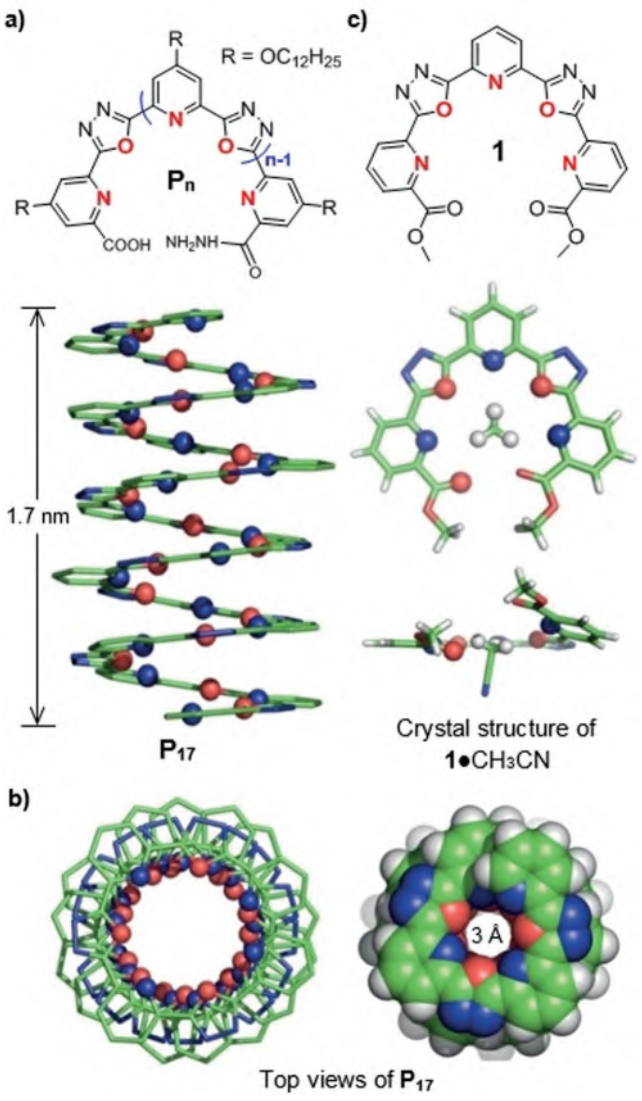


***Figure 1.*** a) Molecular design of helical foldamer channels $\mathbf{P_n}$, such as $\mathbf{P_{17}}$, which contain an average of 17 repeating units computationally determined at the ωB97X/6-31G* level. b) An illustration of the interior cavity, which is ca. 3 Å in diameter after subtracting the van der Waals radius of O (1.52 Å) and N (1.55 Å) nuclei in $\mathbf{P_{17}}$; each helical turn contains ca. 3.4 repeating units and spans a distance of 3.4 Å. c) The structure of trimer **1** and its crystal structure **1**·$CH_3CN$, with an interior cavity of ca. 3.2 Å; atoms involved in H-bonds with H-bonding distances of ≤2.8 Å are highlighted as small balls.

binding energy of 83.3 kcal mol$^{-1}$ that allows all six water molecules around the $K^+$ ion to be stripped; in the case of the $Na^+$ ion, the water molecules are not stripped away (Figures 2a,b). Considering that these ions may also move inside the hollow cavity in the form of $\mathbf{M}^+\cdot(\mathbf{H_2O})_2$ (Figure S2), which ion is transported preferentially still cannot be unambiguously determined on the basis of the size and energy comparisons.

Trimer **1** and pentamer **3** were synthesized following an established two-step synthetic strategy[5i] that involves generating hydrazide-linked trimeric and pentameric molecules and subsequent cyclization of hydrazide groups using $POCl_3$ (Figure 1c; Schemes S1 and S3). The crystal structure of **1** clearly reveals an expected crescent-shaped conformation (Figure 1c), which is reinforced by the differential repulsive interactions among its heteroatoms. The internal cavity was found to be 3.2 Å in diameter—a value that differs slightly from the computationally determined 3 Å. This slightly enlarged cavity can be attributed to the inclusion of one molecule of $CH_3CN$ in the cavity center by three intermolecular H-bonds. The helically folded structure of pentamer **3** was confirmed by the end-to-end nuclear Overhauser enhancement (NOE) contacts seen in the 2D NOESY spectrum (Figures S3–S5).

The aforementioned experimental and computational structural investigations suggest that every helical turn in $\mathbf{P_n}$ with a helical pitch of approximately 3.4 Å comprises about 3.4 repeating units; that is, addition of one repeating unit increases the helical height by 1 Å and thus polymer $\mathbf{P_n}$, comprising an average of n repeating units, has a helical height of n Å. Hinging on the fact that the highly efficient ion-transporting dimeric gA channel only has a height of 25 Å, we reasoned that a helically folded polymer $\mathbf{P_n}$ with 25 or more repeating units (for example, ≥ seven helical turns and ≥ 25 Å in height) would function well in the lipid membrane.

Using the same two-step synthetic strategy (Figure 2c), we searched for polymerization conditions that could lead to $\mathbf{P_{25}}$ or longer polymers. Encouraged by our recent finding that peptide coupling agents enable efficient macrocyclization to form H-bonded rigid aromatic pentamers,[7] we decided to scrutinize the one-pot polymerization efficacies of nine coupling agents. DMF (20% *N*,*N*-dimethylformamide) was added into the reaction solvent ($CH_2Cl_2$) to relax the backbone rigidity enforced by intramolecular H-bonds. During screening of the conditions, an incompletely acidified diacid (**2c**) containing $Na^+$ ions at 29 mol% was used. With it, we found that DEPBT (3-(diethoxyphosphoryl-oxy)-1,2,3-benzotriazin-4(3*H*)-one) is the only coupling agent that enables the efficient production of linear polymers (**LP**) in 64% yield; with a number average molecular weight ($M_n$) of 9.2 kDa that consists of an average of 27 repeating units (referred to as $\mathbf{LP_{27}}$). This gel permeation chromatography (GPC)-derived molecular weight is almost identical to that determined by $^1$H NMR spectroscopy (Figures S6 and S7). All the other eight coupling methods only generate **LP**s of 3.1–5.9 kDa (Table S2). Surprisingly, using completely neutralized diacid **2c**, DEPBT yields the much shorter $\mathbf{LP_{16}}$ (5.5 kDa). Short **LP**s (3.3 to 6.1 kDa) were invariably obtained using seven coupling reagents (Table S2), with the exception of HATU, which produces the relatively long $\mathbf{LP_{23}}$ (8.0 kDa). Such a strong tendency to afford short linear polymers using either $Na^+$-containing or pure diacid **2c** is consistent with a general difficulty in producing long H-bonded aromatic foldamers. Presumably, this arises from the rigidity-induced low reactivities of the reactive groups confined within the H-bond-rigidified backbone. In fact, the one-pot polymerization method has not been very successful to date, and has only given rise to fully H-bonded foldamer channels of ≤ 1.7 nm.[6a]

Linear polymers $\mathbf{LP_{23}}$ and $\mathbf{LP_{27}}$ were cyclized using $POCl_3$ to generate helically folded $\mathbf{P_{23}}$ (2.3 nm) and $\mathbf{P_{27}}$ (2.7 nm). Dehydration of hydrazide (-CONHNHCO-) groups in linear precursors to form cyclic 1,3,4-oxadiazole groups is supported

  

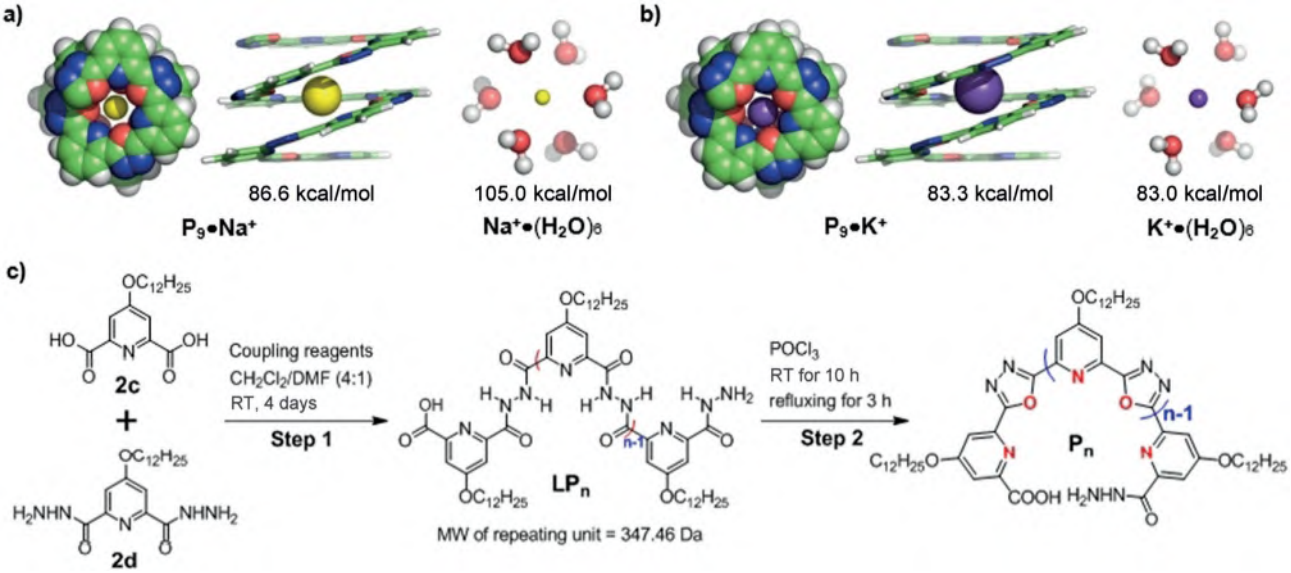


***Figure 2.*** a,b) The computationally determined structures at the level of ωB97X/6-31G* and the corresponding binding energies for $\mathbf{P_9}\cdot\mathbf{Na^+}$, $\mathbf{Na^+}\cdot(\mathbf{H_2O})_6$, $\mathbf{P_9}\cdot\mathbf{K^+}$, and $\mathbf{K^+}\cdot(\mathbf{H_2O})_6$; the single-point energies are calculated at the ωB97X/6-31G + + (2d,p) level. The CPK model of complex $\mathbf{P_9}\cdot\mathbf{Na^+}$ reveals that $Na^+$ ions have an ionic diameter of 2.04 Å that is much smaller than the cavity size of 3 Å, thereby preventing formation of strong coordination bonds with O and N atoms in $\mathbf{P_9}$. c) A two-step synthetic strategy for preparing foldamer channels $\mathbf{P_n}$ with linear polymers $\mathbf{LP_n}$ as the intermediates.

by the complete disappearance of hydrazide protons (9.5–12.0 ppm), which are characteristic of linear polymers (Figure S8). Matrix-assisted laser desorption/ionization time-of-flight (MALDI-TOF) mass spectrometry measurements of $\mathbf{P_{27}}$ are consistent with the polymeric nature of the material (Figure S9).

Fluorescence titrations with 0–20 equivalents of $KPF_6$ or $NaPF_6$ into a chloroform solution of $\mathbf{P_{23}}$ or $\mathbf{P_{27}}$ at 20 μM were conducted (Figures 3 a,b). $K^+$-induced significant fluorescence quenching of the helical backbones were observed for both channels $\mathbf{P_{23}}$ and $\mathbf{P_{27}}$, with much smaller changes by $Na^+$ ions. Specifically, with the intensity in the absence of metal ions set to be 100 %, $K^+$ and $Na^+$ ions resulted in respective fluorescence quenching by 14.3 % and 4.1 % at 365 nm in the case of $\mathbf{P_{23}}$. For $\mathbf{P_{27}}$, the corresponding changes were 11.3 % ($K^+$) and 3.1 % ($Na^+$) at 365 nm. Together with the structural and binding energy data presented in Figures 2 a,b, these differential changes of the same pattern for $\mathbf{P_{23}}$ and $\mathbf{P_{27}}$ indicate that both channels with a narrow hollow cavity may preferentially transport $K^+$ over $Na^+$ ions.

Single-channel current traces recorded in symmetrical (*cis* chamber = *trans* chamber = 1 M KCl) and unsymmetrical

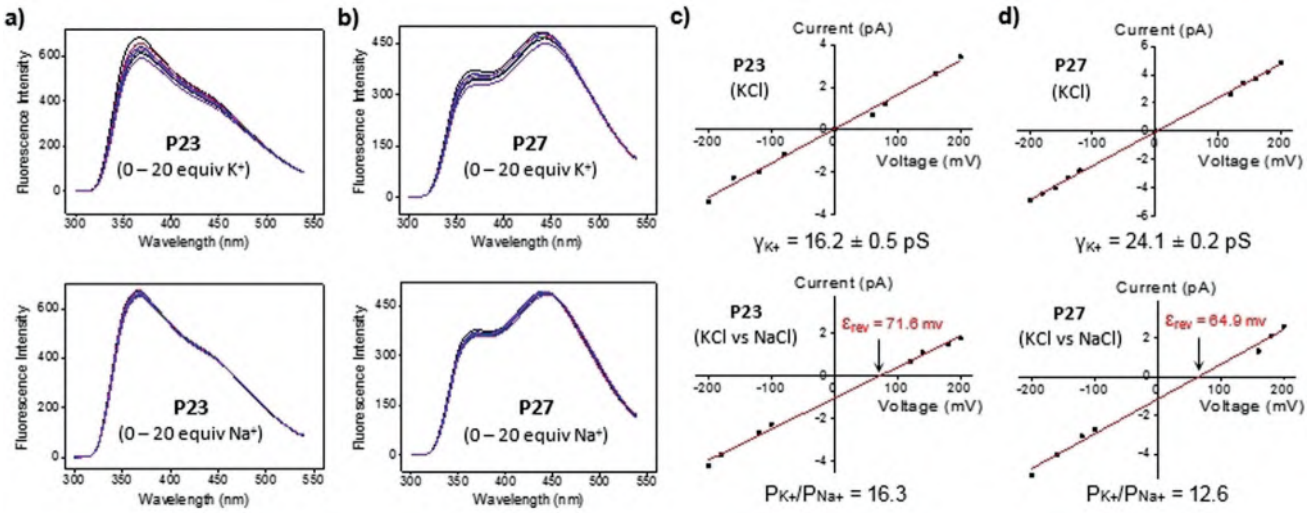


***Figure 3.*** a,b) Changes in the fluorescence intensity of the helical backbone upon titrating 0–20 equiv of $K^+$ or $Na^+$ ions into the chloroform solution of $\mathbf{P_{23}}$ and $\mathbf{P_{27}}$ at 20 μM. c,d) The linear relationships of current traces versus voltages for $\mathbf{P_{23}}$ and $\mathbf{P_{27}}$ in the planar lipid bilayer in symmetrical 1 M KCl solutions (*cis* chamber = *trans* chamber = 1 M KCl, top) and unsymmetrical solutions (*cis* chamber = 1 KCl, *trans* chamber = 1 M NaCl, bottom) for determining the ion conductance value and transport selectivity, respectively.

  

baths (*cis* chamber = 1M KCl, *trans* chamber = 1M NaCl) provide compelling evidence that validates the channel activities of $\mathbf{P_{23}}$ and $\mathbf{P_{27}}$ at the single-channel level (Figures S10–S15). Current traces plotted against voltages yielded both the potassium conduction rate ($\gamma_{K+}$) and the ion selectivity ratio ($P_{K+}/P_{Na+}$) for these two channels (Figures 3c,d). The determined conductance values of $16.2 \pm 0.5$ pS for $\mathbf{P_{23}}$ and $24.1 \pm 0.2$ pS for $\mathbf{P_{27}}$, which are comparable to $23.2 \pm 0.4$ pS obtained for the gramicidin A channel,[3i] confirm the high activity of $\mathbf{P_n}$-mediated transport of $K^+$ ions. Significantly, on the basis of the determined reverse potential values ($\varepsilon_{rev}$, Figures 3c,d; Figures S11 and S15) and $\varepsilon_{rev} = RT/F \times \ln(P_{K}{}^{+}/P_{Na}{}^{+})$ (the universal gas constant $R = 8.314\ J\,K^{-1}\,mol^{-1}$, $T = 300$ K, Faraday's constant $F = 96485\ C\,mol^{-1}$, and $P$ is the ion permeability), $K^{+}/Na^{+}$ selectivities for $\mathbf{P_{23}}$ and $\mathbf{P_{27}}$ were calculated to be 16.3 and 12.6, respectively, which are exceptionally high among synthetic ion channels.[2g,h,3]

An inverse correlation between conductance and selectivity is likely to exist as less selective channels transport ions at a faster speed. This can be reasonably explained on the basis of the channel length and the hydrophobic thickness (ca. 2.6 nm) of the lipid bilayer membrane formed by diPhyPC (1,2-diphytanoyl-*sn*-glycero-3-phosphocholine),[8] which is employed for single-channel current measurement. On the one hand, $\mathbf{P_{27}}$ (2.7 nm long) can fully span the hydrophobic membrane region and therefore mediate faster ion transport, with selectivity largely determined by the channel's own intrinsic differential tendencies in ion transport. On the other hand, $\mathbf{P_{23}}$ (average channel length of 2.3 nm) is too short to fully span the 2.6 nm hydrophobic membrane region, and ion transport becomes slower. Compared to $Na^+$ ions, $K^+$ ions are more permeable to a hydrophobic path of 0.3 nm because they are either softer in nature or require a lower dehydration energy per water molecule (13.8 kcal mol$^{-1}$ for $K^+$ versus 17.5 kcal mol$^{-1}$ for $Na^+$; Figures 2a,b); therefore, the ion transport selectivity is higher for $\mathbf{P_{23}}$.

Lastly, $\mathbf{P_{23}}$-mediated transport selectivities toward $Rb^+$ and $Cs^+$ ions were also measured (Figures S12–S13), with $K^+/Rb^+ = 0.25$ and $K^+/Cs^+ = 1.6$. Given that $\mathbf{P_{23}}$ possesses a hollow cavity that is 3 Å in diameter, the observed ion transport selectivity trend of $Rb^+ > K^+ > Cs^+ > Na^+$ agrees with the ionic diameters of $Cs^+$ (3.34 Å), $Rb^+$ (3.04 Å), $K^+$ (2.76 Å), and $Na^+$ (2.04 Å). $\mathbf{P_9}$ provides a sufficient binding energy of 84.11 kcal mol$^{-1}$ to strip off all six water molecules around the $Rb^+$ ion (Figure S16). Additionally, the fact that the larger $Cs^+$ ions can be efficiently transported suggests that the channel cavity has a dynamic nature that is able to adapt and accommodate larger ions. This is consistent with the crystal structure of trimer **1** (Figure 1c), which demonstrates an increase in internal cavity up to 3.2 Å in the presence of a guest molecule (acetonitrile) compared to the computationally determined diameter of 3 Å without a guest.

To summarize, by screening various types of coupling agents, we serendipitously discovered a combination of $Na^+$-containing diacid and DEPBT as a powerful one-pot polymerization method. This allows for the rapid and efficient one-pot preparation of H-bonded linear polyhydrazides, which are sufficiently long to helically fold into foldamer-based channels of approximately 2.7 nm in length after backbone cyclization mediated by $POCl_3$. To our best knowledge, this is the fifth type of aromatic foldamer-based helical channels of $> 2.0$ nm made by one-pot polymerization, following on from four seminal reports by other researchers,[5h,j,6b,c] and it is the second demonstration of the impressive ion-transporting potential of aromatic foldamer-based channels after the work by Dong.[5j] Specific to our current work, the helical channels ($\mathbf{P_{23}}$ and $\mathbf{P_{27}}$), containing a narrow hollow cavity of 3 Å decorated by helically arranged O and N atoms along the hollow helix, exhibit highly active and exceptionally selective transport of $K^+$ ions with respect to $Na^+$ ions. In particular, $\mathbf{P_{23}}$ is 2.3 nm long and displays an exceptionally high $K^+/Na^+$ selectivity of 16.3. Further refinement of the one-pot polymerization method may give rise to longer foldamer channels for other interesting applications.

## Acknowledgements

This work is supported by the NanoBio Lab (Biomedical Research Council, Agency for Science, Technology and Research, Singapore).

## Conflict of interest

The authors declare no conflict of interest.

**Keywords:** covalent organic nanotubes · hydrogen bonds · ion transport · polyhydrazides · supramolecular chemistry

**How to cite:** *Angew. Chem. Int. Ed.* **2020**, *59*, 1440–1444
*Angew. Chem.* **2020**, *132*, 1456–1460

[1] a) P. Agre, *Proc. Am. Thorac. Soc.* **2006**, *3*, 5; b) K. Murata, K. Mitsuoka, T. Hirai, T. Walz, P. Agre, J. B. Heymann, A. Engel, Y. Fujiyoshi, *Nature* **2000**, *407*, 599; c) E. Tajkhorshid, P. Nollert, M. Ø. Jensen, L. J. W. Miercke, J. O'Connell, R. M. Stroud, K. Schulten, *Science* **2002**, *296*, 525; d) D. A. Doyle, J. Morais Cabral, R. A. Pfuetzner, A. Kuo, J. M. Gulbis, S. L. Cohen, B. T. Chait, R. MacKinnon, *Science* **1998**, *280*, 69; e) J. A. Mould, H.-C. Li, C. S. Dudlak, J. D. Lear, A. Pekosz, R. A. Lamb, L. H. Pinto, *J. Biol. Chem.* **2000**, *275*, 8592.

[2] a) A. P. Davis, D. N. Sheppard, B. D. Smith, *Chem. Soc. Rev.* **2007**, *36*, 348; b) J. T. Davis, O. Okunola, R. Quesada, *Chem. Soc. Rev.* **2010**, *39*, 3843; c) A. Vargas Jentzsch, A. Hennig, J. Mareda, S. Matile, *Acc. Chem. Res.* **2013**, *46*, 2791; d) N. Sakai, S. Matile, *Langmuir* **2013**, *29*, 9031; e) J. Montenegro, M. R. Ghadiri, J. R. Granja, *Acc. Chem. Res.* **2013**, *46*, 2955; f) T. M. Fyles, *Acc. Chem. Res.* **2013**, *46*, 2847; g) F. Otis, M. Auger, N. Voyer, *Acc. Chem. Res.* **2013**, *46*, 2934; h) G. W. Gokel, S. Negin, *Acc. Chem. Res.* **2013**, *46*, 2824; i) Y. Zhao, H. Cho, L. Widanapathirana, S. Zhang, *Acc. Chem. Res.* **2013**, *46*, 2763; j) B. Gong, Z. Shao, *Acc. Chem. Res.* **2013**, *46*, 2856; k) Y. P. Huo, H. Q. Zeng, *Acc. Chem. Res.* **2016**, *49*, 922; l) R. H. Tunuguntla, F. I. Allen, K. Kim, A. Belliveau, A. Noy, *Nat. Nanotechnol.* **2016**, *11*, 639; m) S. Howorka, *Nat. Nanotechnol.* **2017**, *12*, 619; n) J.-Y. Chen, J.-L. Hou, *Org. Chem. Front.* **2018**, *5*, 1728.

[3] a) Y. Tanaka, Y. Kobuke, M. Sokabe, *Angew. Chem. Int. Ed. Engl.* **1995**, *34*, 693; *Angew. Chem.* **1995**, *107*, 717; b) Y. Kobuke, T. Nagatani, *J. Org. Chem.* **2001**, *66*, 5094; c) G. W. Gokel, A.

  

Mukhopadhyay, *Chem. Soc. Rev.* **2001**, *30*, 274; d) C. D. Hall, G. J. Kirkovits, A. C. Hall, *Chem. Commun.* **1999**, 1897; e) N. Sakai, D. Gerard, S. Matile, *J. Am. Chem. Soc.* **2001**, *123*, 2517; f) Z. Sun, M. Barboiu, Y.-M. Legrand, E. Petit, A. Rotaru, *Angew. Chem. Int. Ed.* **2015**, *54*, 14473; *Angew. Chem.* **2015**, *127*, 14681; g) A. Gilles, M. Barboiu, *J. Am. Chem. Soc.* **2016**, *138*, 426; h) C. Lang, X. Deng, F. Yang, B. Yang, W. Wang, S. Qi, X. Zhang, C. Zhang, Z. Dong, J. Liu, *Angew. Chem. Int. Ed.* **2017**, *56*, 12668; *Angew. Chem.* **2017**, *129*, 12842; i) C. L. Ren, J. Shen, H. Q. Zeng, *J. Am. Chem. Soc.* **2017**, *139*, 12338; j) M. Barboiu, *Acc. Chem. Res.* **2018**, *51*, 2711; k) P. Xin, H. Kong, Y. Sun, L. Zhao, H. Fang, H. Zhu, T. Jiang, J. Guo, Q. Zhang, W. Dong, C.-P. Chen, *Angew. Chem. Int. Ed.* **2019**, *58*, 2779; *Angew. Chem.* **2019**, *131*, 2805; l) R. J. Ye, C. L. Ren, J. Shen, N. Li, F. Chen, A. Roy, H. Q. Zeng, *J. Am. Chem. Soc.* **2019**, *141*, 9788 – 9792.

[4] a) D. J. Hill, M. J. Mio, R. B. Prince, T. S. Hughes, J. S. Moore, *Chem. Rev.* **2001**, *101*, 3893; b) D.-W. Zhang, X. Zhao, J.-L. Hou, Z.-T. Li, *Chem. Rev.* **2012**, *112*, 5271; c) H. L. Fu, Y. Liu, H. Q. Zeng, *Chem. Commun.* **2013**, *49*, 4127; d) Y. Ferrand, I. Huc, *Acc. Chem. Res.* **2018**, *51*, 970.

[5] a) Y. Hamuro, S. J. Geib, A. D. Hamilton, *Angew. Chem. Int. Ed. Engl.* **1994**, *33*, 446; *Angew. Chem.* **1994**, *106*, 465; b) J. Zhu, R. D. Parra, H. Q. Zeng, E. Skrzypczak-Jankun, X. C. Zeng, B. Gong, *J. Am. Chem. Soc.* **2000**, *122*, 4219; c) V. Berl, I. Huc, R. G. Khoury, M. J. Krische, J. M. Lehn, *Nature* **2000**, *407*, 720; d) J. C. Nelson, J. G. Saven, J. S. Moore, P. G. Wolynes, *Science* **1997**, *277*, 1793; e) R. A. Smaldone, J. S. Moore, *J. Am. Chem. Soc.* **2007**, *129*, 5444; f) G. S. Hanan, J.-M. Lehn, N. Kyritsakas, J. Fischer, *J. Chem. Soc. Chem. Commun.* **1995**, 765; g) L. A. Cuccia, J.-M. Lehn, J.-C. Homo, M. Schmutz, *Angew. Chem. Int. Ed.* **2000**, *39*, 233; *Angew. Chem.* **2000**, *112*, 239; h) J.-L. Schmitt, J.-M. Lehn, *Helv. Chim. Acta* **2003**, *86*, 3417; i) J. Zhu, Z. Dong, S. Lei, L. Cao, B. Yang, W. Li, Y. Zhang, J. Liu, J. Shen, *Angew. Chem. Int. Ed.* **2015**, *54*, 3097; *Angew. Chem.* **2015**, *127*, 3140; j) C. Lang, W. Li, Z. Dong, X. Zhang, F. Yang, B. Yang, X. Deng, C. Zhang, J. Xu, J. Liu, *Angew. Chem. Int. Ed.* **2016**, *55*, 9723; *Angew. Chem.* **2016**, *128*, 9875; k) C. L. Ren, V. Maurizot, H. Q. Zhao, J. Shen, F. Zhou, W. Q. Ong, Z. Y. Du, K. Zhang, H. B. Su, H. Q. Zeng, *J. Am. Chem. Soc.* **2011**, *133*, 13930; l) B. Gong, H. Q. Zeng, J. Zhu, L. H. Yuan, Y. H. Han, S. Z. Cheng, M. Furukawa, R. D. Parra, A. Y. Kovalevsky, J. L. Mills, E. Skrzypczak-Jankun, S. Martinovic, R. D. Smith, C. Zheng, T. Szyperski, X. C. Zeng, *Proc. Natl. Acad. Sci. USA* **2002**, *99*, 11583.

[6] a) D.-W. Zhang, H. Wang, Z.-T. Li, *Macromol. Rapid Commun.* **2017**, *38*, 1700179; b) S. Hecht, A. Khan, *Angew. Chem. Int. Ed.* **2003**, *42*, 6021; *Angew. Chem.* **2003**, *115*, 6203; c) K. Maeda, L. Hong, T. Nishihara, Y. Nakanishi, Y. Miyauchi, R. Kitaura, N. Ousaka, E. Yashima, H. Ito, K. Itami, *J. Am. Chem. Soc.* **2016**, *138*, 11001.

[7] Z. Y. Du, C. L. Ren, R. J. Ye, J. Shen, Y. J. Lu, J. Wang, H. Q. Zeng, *Chem. Commun.* **2011**, *47*, 12488.

[8] C. Potrich, H. Bastiani, D. A. Colin, S. Huck, G. Prevost, M. Dalla Serra, *J. Membr. Biol.* **2009**, *227*, 13.

Manuscript received: May 22, 2019
Revised manuscript received: September 18, 2019
Accepted manuscript online: October 4, 2019
Version of record online: November 19, 2019

  